Key Points:

- A unique 1 year stratiform cloud data set was obtained for the Amazon Basin
- During the dry season, ice forms more efficient than during the wet season
- Biomass burning aerosols must be the source of ice nuclei during the dry season

Correspondence to:
P. Seifert,
seifert@tropos.de

Seasonal variability of heterogeneous ice formation in stratiform clouds over the Amazon Basin

Patric Seifert[1], Clara Kunz[1], Holger Baars[1], Albert Ansmann[1], Johannes Bühl[1], Fabian Senf[1], Ronny Engelmann[1], Dietrich Althausen[1], and Paulo Artaxo[2]

[1]Leibniz Institute for Tropospheric Research, Leipzig, Germany, [2]Institute of Physics, University of São Paulo, São Paulo, Brazil

Abstract Based on 11 months of polarization lidar observations in the Amazon Basin near Manaus, Brazil (2.3°S, 60°W), the relationship between temperature and heterogeneous ice formation efficiency in stratiform clouds was evaluated in the cloud top temperature range between −40 and 0°C. Between −30 and 0°C, ice-containing clouds are a factor of 1.5 to 2 more frequent during the dry season. Free-tropospheric aerosol backscatter profiles revealed a twofold to tenfold increase in aerosol load during the dry season and a Monitoring Atmospheric Composition and Climate — Interim Implementation reanalysis data set implies that the aerosol composition during the dry season is strongly influenced by biomass burning aerosol, whereas other components such as mineral dust do not vary strongly between the seasons. The injection of smoke accompanied by the likely dispersion of biological material, soil dust, or ash particles was identified as a possible source for the increased ice formation efficiency during the dry season.

1. Introduction

The Amazon Basin is considered as one of the tipping elements of Earth's climate system, but little is known on the interaction of its unique ecosystem with meteorological processes [*Lenton et al.*, 2008]. The biological activity over the forest is responsible for the emissions of primary biological particles as well as the emission of volatile organic compounds that form secondary organic aerosol particles [*Artaxo et al.*, 2013]. The human activity in the Amazon Basin produces a variety of local aerosols that provide the nuclei for cloud droplets and ice crystals [*Martin et al.*, 2010] whose properties are important in the formation of precipitation. Another source of aerosols over the Amazon Basin is long-range transport of mineral dust and biomass burning smoke from the African continent [*Baars et al.*, 2011] that also contribute to the local population of cloud droplet and ice nuclei [*Prenni et al.*, 2009; *Pöschl et al.*, 2010].

One key component for the production of significant amounts of precipitation is the formation of ice crystals that are required to produce sufficiently large hydrometeors via the cold rain process [*Korolev and Mazin*, 2003]. It is well known that in particular the efficiency of heterogeneous ice nucleation that occurs at temperatures between −37 and 0°C depends strongly on the type of ice nucleating particle (INP), i.e., the aerosol type, as well on the humidity and temperature of the atmosphere [*Hoose and Möhler*, 2012; *Murray et al.*, 2012; *DeMott et al.*, 2015]. Under otherwise constant conditions variations in the aerosol properties can therefore affect the microphysical structure of clouds, which had been observed previously [*Sassen et al.*, 2003; *Seifert et al.*, 2010; *Kanitz et al.*, 2011; *Zhang et al.*, 2012].

In this study, we present a lidar-based statistical analysis of the occurrence of heterogeneous ice formation in stratiform cloud layers that were observed near Manaus, Brazil, between January and November 2008 — thus covering both the wet and the dry season. The lidar observations provide the unique chance to evaluate possible effects of the seasonal variation of the aerosol properties on the efficiency of heterogeneous ice formation under ambient conditions over the Amazon Basin. In section 2 the observational principle and the methodology are presented. Results of the analysis of the mixed-phase cloud data set are presented in section 3. In section 4 the findings are summarized and concluded.

2. Experiment and Methodology
2.1. Experiment

Between January and November 2008, continuous observations with the Raman polarization lidar Polly[XT] [*Althausen et al.*, 2009] were carried out 60 km north of Manaus, Brazil (2.3°S, 60°W) in the framework

of EUCAARI (European Integrated Project on Aerosol, Cloud, Climate, Air Quality Interactions) [*Kulmala et al.*, 2011] and Amazonian Aerosol Characterization Experiment 2008 [*Martin et al.*, 2010]. The lidar measurements were analyzed previously with respect to the aerosol conditions present in the lower troposphere during the wet and dry season by *Baars et al.* [2012], who report that the dry season features a much higher aerosol load, predominantly caused by biomass burning aerosol.

2.2. Identification of Cloud Layers

Besides the vertical structure of the aerosol profile, cloud layers were observed frequently during the measurement period. The observed cloud layers were classified as either ice containing or pure liquid in accordance to the methodology applied previously by *Ansmann et al.* [2009], *Seifert et al.* [2010, 2011], and *Kanitz et al.* [2011]. Here the procedure is thus only explained briefly. We define a single cloud layer when it is separated from adjacent ones by 500 m in the vertical and by 5 min in time. If the vertical or temporal distance between two layers is less, they are defined as one layer. Above the apparent top of the cloud layer the lidar signal-to-noise ratio must be at least 3% above the background noise level of the average cloud-containing profile. This requirement ensures that the data set contains only cloud layers that could be penetrated by the lidar beam in order to obtain an accurate measure of the cloud top height. In the next step, the depolarization ratio profile is obtained for the identified cloud layer. Hereby, layers containing ice crystals can be identified by means of an increased depolarization ratio when being observed by an off-zenith-pointing lidar as it is the case for Polly^{XT} (pointing 5° off zenith). Spherical particles, such as cloud droplets, do not produce depolarization. Nevertheless, a cloud layer is only identified as ice-containing when increased values of depolarization are observed at its very base (including potential ice virgae), as multiple scattering in liquid cloud layers can also cause a linear increase of the depolarization with increasing cloud penetration depth. Because lidar can only penetrate optical depths of up to 3 and we require that the signal is not attenuated above a cloud layer, the data set is restricted to thin stratiform cloud layers, similar to those identified in a satellite-based study of *Zhang et al.* [2012]. The cloud layers did not necessarily have to contain a liquid layer at top. Thus, the class of ice-containing clouds also comprises cirrus clouds. It is known that temperature is the main parameter controlling the efficiency of heterogeneous ice nucleation [*DeMott et al.*, 2015]. Hence, the temperature at the top of every identified cloud layer is obtained from GDAS1 data that are based on the global data assimilation system GDAS (Global Data Analysis System, http://ready.arl.noaa.gov/gdas1.php, grid point: $x = 301$, $y = 88$). *Seifert et al.* [2010] and *Kanitz et al.* [2011] evaluated the accuracy of GDAS1 data against collocated atmospheric soundings and found a mean standard deviation of less than 1 K for the middle troposphere where the mixed-phase clouds are usually observed.

2.3. Determination of Aerosol Profiles

The direct observation of the aerosol properties in the vicinity of each cloud layer is difficult to archive because often the presence of surrounding or lower cloud layers prohibit the determination of a cloud-free backscattering profile from the lidar measurement. The approach to characterize the aerosol properties in the free troposphere was thus twofold. First, the Polly^{XT} data set presented previously by *Baars et al.* [2012] was screened for upper level clouds to obtain the aerosol optical properties for the upper troposphere. Second, reanalysis data of the Monitoring Atmospheric Composition and Climate — Interim Implementation (MACC) was obtained for nine grid points surrounding the observation site (central MACC grid point: 2.25°S, 60.75°W). The MACC data set provides profiles of the mass mixing ratio of mineral dust for three size intervals (0.03–0.55 μm, 0.55–0.9 μm, and 0.9–20 μm radius), sea salt for three size intervals (0.03–0.5 μm, 0.5–5 μm, and 5–20 μm radius), hydrophilic black carbon, hydrophobic black carbon, hydrophilic organic matter, and sulfate aerosol at 60 model levels with a temporal resolution of 6 h and a horizontal resolution of 0.75° [*Morcrette et al.*, 2009].

In the present study, we use the profiles of backscatter coefficient to depict differences in the aerosol load between the wet and dry season. The MACC aerosol reanalysis will provide indications for changes in the aerosol mixture.

3. Results

3.1. Mixed-Phase Cloud Statistics

The total 11 month data set of Polly^{XT} measurements in Amazonia covers 2100 measurement hours. The measurements were regularly paused around solar noon and in the afternoon. The breaks lasted from 3 to 6.5 h between 1100 and 1730 local time, 1500–2130 UTC, to prevent damage of the lidar detectors by direct

Table 1. Overview on the Extent of the Manaus Cloud Data Set Separately for the Dry Season (January–June 2008) and Wet Season (July–November 2008), Respectively, for the Full Data Set and for the Subdata Set Covering the Heterogeneous Freezing Range With $-40 \leq T_{top} \leq 0°C$[a]

Parameter	Wet Season	Dry Season
All identified clouds	1480 (683)	659 (377)
WD clouds	885 (447)	321 (213)
WD liquid clouds	646 (326)	124 (84)
WD ice clouds	239 (121)	197 (129)
All clouds: $-40 \leq T_{top} \leq 0°C$	507 (261)	204 (132)
WD clouds: $-40 \leq T_{top} \leq 0°C$	314 (176)	139 (100)
WD liquid clouds: $-40 \leq T_{top} \leq 0°C$	230 (135)	58 (45)
WD ice clouds: $-40 \leq T_{top} \leq 0°C$	84 (41)	81 (55)

[a]The values in parentheses denote the number of cases observed during nighttime between 22 and 10 UTC. WD: well-defined (cloud top could be determined). Ice clouds also comprise mixed-phase clouds.

sunlight hitting the lidar telescope and to extend the life time of the laser lash lamps. During rain the lidar also turned off automatically and occasionally the lidar was off for maintenance.

Table 1 presents the main numbers of the data set separately for the dry season (January–June 2008) and wet season (July–November 2008). The values in parentheses denote the number of respective nighttime observations. Partly in multiple layers, 2139 cloud layers were observed with a total occurrence time of 2200 h. Approximately 40% of the observed clouds (993) could not be penetrated due to too high optical depth. The remaining ones (1206) were classified to be well defined (WD). The wet season features much more liquid clouds than the dry season. The number of observed ice-containing clouds is approximately constant during both seasons. From the 711 cloud layers observed in the temperature range between -40 and $0°C$, 453 stratiform well-defined clouds with detectable cloud top were identified. Considerably, more clouds were observed during the wet season (314 versus 139) which is a consequence of the different atmospheric conditions during both seasons. During the dry season, most clouds were observed at night because the lidar was usually turned off for 5–6 h during daytime. When the number of clouds observed at $-40 \leq T \leq 0°C$ is compared to the full data set, it can be seen that most liquid clouds occur at $T > 0°C$ and that most ice-containing clouds occur at $T < -40°C$, which is outside the temperature range of heterogeneous freezing.

Figure 1 presents the fraction of well-defined ice-containing clouds as a function of cloud top temperature between -40 and $0°C$ for intervals of 5 K. For the full temperature range of heterogeneous freezing, it can be seen that the fraction of ice-containing clouds observed during the dry season is considerably higher than during the wet season. At temperatures above $-20°C$, the absolute number of ice-containing clouds is rather low. Nevertheless, during the dry season the freezing efficiency exceeds the one of the wet season by about a factor of 2. For example, between -10 and $-20°C$, 20% of all clouds observed during the wet season contained ice whereas it were approximately 40% during the dry season. With decreasing temperature, the relative difference in the fraction of ice-containing clouds decreases as the total amount of ice-containing clouds increases. At temperatures below $-30°C$, all clouds observed during the dry season contained ice, which was also the case during the
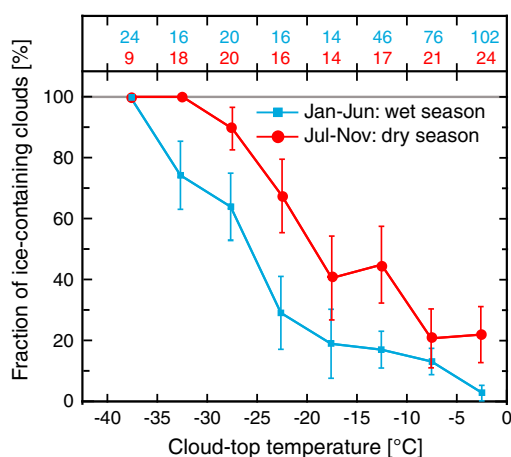

Figure 1. Fraction of ice-containing clouds as function of cloud top temperature in intervals of 5 K for the wet (blue) and dry season (red). Number of clouds per interval is shown in the header. Error bars indicate the statistical uncertainty [*Seifert et al.*, 2010].
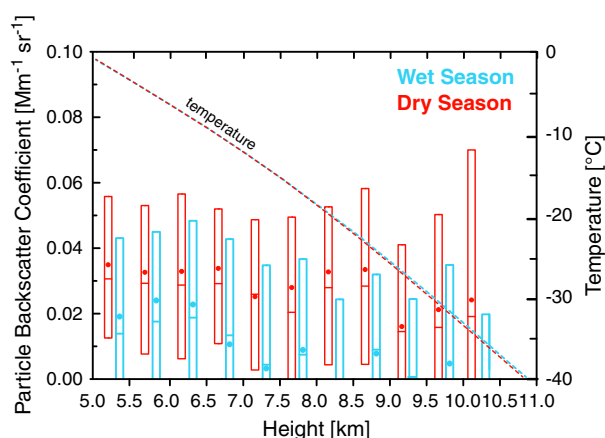
Figure 2. Mean (circles), median (center of boxes), and 25/75 percentiles (bottom and top of boxes) of the particle backscatter coefficient at 532 nm wavelength for the wet and dry season obtained from Polly[XT] observations as described in *Baars et al.* [2012]. Mean GDAS1 temperature profiles for both seasons are shown in addition.

wet season when temperatures were below −35°C. With respect to the statistical error shown by the error bars (see *Seifert et al.* [2010] for details), the difference in freezing efficiency between dry and wet season can be considered to be significant throughout the investigated temperature range. In addition to the statistics shown in Figure 1, tests were performed to check the consistency of the cloud data set. First, as was also done by *Seifert et al.* [2010], we checked the response of the statistics to seeding effects, which can occur when sedimenting ice crystals from an upper level ice-containing cloud trigger ice formation in a supercooled liquid clou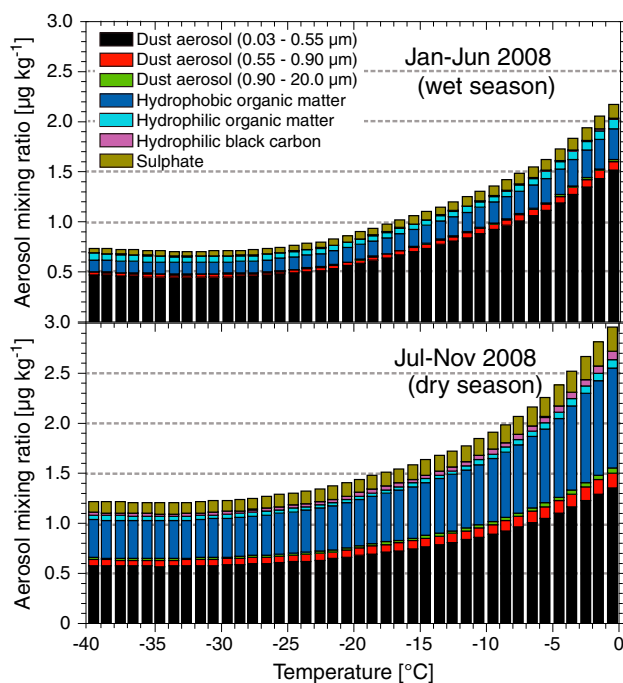d beneath that otherwise would have not formed ice. Second, also the clouds with undetermined cloud top were incorporated in the statistical analysis (assuming that the highest data point with signal above the background level is the apparent cloud top). Third, we analyzed the data set separately for daytime and nighttime cases to check for daylight effects on the lidar measurements. The three tests revealed similar differences in the ice-containing cloud fraction between wet and dry season as is shown in Figure 1.

It should be noted that ice formation does not necessarily need to be completely absent when no ice signatures are observed with polarization lidar. As *Bühl et al.* [2013] point out, the optical extinction and correspondingly the backscatter signal of ice crystals is very low for low crystal concentrations as they are produced at rather high temperatures of above −10°C. The detection threshold with respect to ice water content lies approximately in the range of 1×10^{-6} kg m^{-3}. Consequently, the increase in the fraction of ice-containing clouds between the wet and the dry season can be interpreted as a respective increase in the ice water content resulting from an increase in the number of ice nuclei. This would be in agreement to a satellite-based study of *Zhang et al.* [2012], who found that the ice water path produced by clouds with cloud top temperatures between −15 and −25°C embedded in mineral dust is up to 11.5×10^{-3} kg m^{-2} larger than in clouds not embedded into dust layers. Nevertheless, as *Bühl et al.* [2013] discussed, the lidar-based findings of freezing thresholds are in good agreement to the onset temperatures of ice formation reported in laboratory studies.

3.2. Vertical Structure of Aerosol Properties

In order to evaluate the relationship between the efficiency of heterogeneous ice production and the ambient aerosol conditions, the vertical distribution of aerosol properties in the Manaus area are depicted in the following.

First, measurements of the particle backscatter coefficient measured with Polly[XT] at 532 nm wavelength are investigated. In Figure 2, box plots of the mean profiles of wet and dry season, respectively, for the height range from 5 to 10.5 km are shown. The seasonal mean GDAS1 temperature profiles are shown in addition. It can be seen that the mean temperature profiles are similar for wet and dry season. Median and mean values of the particle backscatter coefficient are similar indicating that the data points are evenly distributed and only few extreme scenarios were observed. Nevertheless, a rather large variability of the observed backscatter coefficients is indicated by the wide range of data points covered by the 25%/75% percentiles, depicted by the boxes. Besides the observed variability, mean and median values are constantly larger during the dry season. At heights above 6.5 km (−10°C), backscatter coefficients obtained for the dry season exceed the respective wet-season values by a factor of 2 to 10. As was shown by *Seifert et al.* [2011], an increase in backscatter coefficient will scale linearly with the number of ice nuclei for otherwise constant aerosol properties.

Figure 3. Seasonal profiles of aerosol mass mixing ratio of seven different aerosol species taken from the MACC reanalysis averaged over nine grid points closest to the observation site.

Taking this assumption granted, the INP concentration during the dry season will exceed the wet-season values by a factor of 2 to 10.

The very low background values of the aerosol particle backscatter coefficient above the lidar site do not allow to infer further information on the particle type from the available lidar measurements, such as particle depolarization ratio or extinction coefficient. We thus use the reanalysis of the vertical profiles of the mixing ratio of different aerosol types modeled by MACC to estimate the seasonal variability of the presence of different main aerosol types. Figure 3 presents the vertical profiles for the temperature range between −40 and 0°C. Overall, it can be seen that the aerosol load during the dry season is calculated to exceed the values for the wet season at all temperature levels. Two main features are visible. First, the total dust aerosol load is similar for both seasons. During the dry season, however, more dust mass is contained in the size ranges from 0.55–20 μm. Second, the mass mixing ratio of hydrophobic organic matter, hydrophilic organic matter, and sulfate is considerably increased during the dry season.

The approximately threefold increase in the mixing ratio of hydrophobic organic matter observed during the dry season can be attributed to increased biomass burning activity. According to *Morcrette et al.* [2009], the sources of sulfates and carbon in the model are linked to fire emissions, both natural and anthropogenic, plus emissions from domestic, industrial, power generation, transport, and shipping activities. Due to its low ice nucleation efficiency [*Hoose and Möhler*, 2012], an increase in black carbon cannot solely explain the observed increase in the ice-containing cloud fraction. It should, however, be noted that emissions of much more ice-nucleation-efficient mineral dust particles in MACC are not related to fire emissions [*Morcrette et al.*, 2009], even though it is known that considerable amounts of mineral dust are emitted during fire events. From polarization Raman lidar measurements in Cyprus it was, for example, concluded that mineral dust contributes 10–50% to the optical extinction of smoke plumes, corresponding to a contribution between 25 and 80% to the aerosol mass [*Nisantzi et al.*, 2014]. Measurements of the dust fraction in lofted Amazonian biomass burning plumes were not reported yet, but surface in situ observations in the Amazon Basin analyzed by *Arana et al.* [2014] suggest that the dust fraction is lower in that region than over Cyprus. For both the dry and wet season, observations in the vicinity of biomass burning activity yield a soil dust fraction of approximately 4% of the total particulate mass and a fraction between soil dust and black carbon of 50–60%. These ratios are constant between both seasons, but the absolute particulate mass and thus the soil dust mass reported by *Arana et al.* [2014] was 4–5 times larger during the dry season than during the wet season (38.5 μg m⁻³ versus 8.7 μg m⁻³). In accordance to *Martin et al.* [2010], *Arana et al.* [2014] relate the major fraction of the observed coarse-mode aerosol (PM_{10}) to primary biological emissions. In the vicinity to biomass burning, respective values of PM_{10} for the dry season were found to be a factor of 1.5 higher than during the wet season. Similar measurements in a pristine environment without nearby biomass burning activity revealed slightly lower values of coarse-mode aerosol and thus reduced primary biological emissions during the dry season. Also, soil dust concentrations reach rarely more than 2% of the total particulate matter at the pristine site. During the wet season, enhanced values of soil dust are only observed when the position of the intertropical

convergence zone is located south of Manaus, allowing long-range transport of dust from Africa [*Baars et al.*, 2011; *Arana et al.*, 2014].

Ashes are another byproduct of biomass burning activity. Their ice nucleation efficiency is considered to be similar to those of mineral dusts. *Umo et al.* [2015] investigated the ice nucleation of four different types of combustion ashes. They identified wood burning ash as the most efficient type, being the second most efficient nonbiological INP, only exceeded by feldspar. Little is known on the actual contribution of ash to the total aerosol mix over the Amazon Basin. For example, *Arana et al.* [2014] did not infer ash fractions from their mass spectrometer measurements discussed above. Also within MACC, ash is only comprised in the black carbon aerosol. Thus, similar to the consideration of soil dust emissions, biomass burning can also lead to the formation and emission of ash that can enhance ice nucleation efficiency during the dry season.

In conclusion, during the dry season, the absolute concentration of soil dust in the vicinity to biomass burning areas can be considered to be 4–5 times higher than during the wet season. Also, the fraction of coarse-mode aerosol, which likely stems from biological emissions, is enhanced in this region. In regions farther away from biomass burning activities, the soil dust fraction as well as the coarse-mode fraction, i.e., primary biological emissions, observed during the wet season, are lower compared to the dry season. Nevertheless, the observations and MACC reanalysis show that during the dry season both fractions of organic material and of mineral dust increase considerably at all tropospheric height levels. It was in addition reported by *Arana et al.* [2014] that frequently deep-convective activity caused transport of the biomass burning aerosol into the free troposphere. With increased concentration of organic matter, dust, and ashes, the dry season is likely to provide populations of more efficient ice nuclei besides black carbon [*Hoose and Möhler*, 2012; *Augustin et al.*, 2013; *Hartmann et al.*, 2013]. Due to missing emission schemes for these by-products of biomass burning, it remains, however, unknown to what extent fire-induced soil dust and ash injection can influence the aerosol conditions at cloud-forming height levels.

4. Conclusions

In the present study the seasonal variability of heterogeneous ice production in thin, stratiform cloud layers with lidar-detectable cloud tops over the Amazon Basin was investigated based on a unique interseasonal continuous polarization lidar data set obtained near Manaus, Brazil. Thin stratiform cloud layers are best suited for studies of primary heterogeneous ice formation in relationship to temperature and aerosol properties because secondary ice formation and ice multiplication processes are inefficient in such clouds. It is also noteworthy that heterogeneous ice formation at $T > -25°C$ was found to occur only via the liquid phase [*Ansmann et al.*, 2009; *Westbrook and Illingworth*, 2011; *de Boer et al.*, 2011]. Thus, potential seasonal differences in the humidity profiles, which could affect the ice supersaturation and, consequently, the efficiency of deposition or condensation freezing nucleation [*Hoose and Möhler*, 2012], cannot explain differences in ice nucleation efficiency at $T > -25°C$.

From the Manaus cloud data set, it was found that at all temperatures between 0 and $-40°C$, ice formed considerably more frequent during the dry season than during the wet season. Differences in the aerosol conditions between both seasons were found as well. During the dry season, the aerosol backscatter coefficient at 532 nm wavelength exceeds the respective wet-season values by a factor of 2 to 10 at all heights between 4 and 10 km. According to MACC reanalysis data, carbon emissions contribute mostly to the enhanced aerosol load observed during the dry season. Thus, based on the data sets analyzed in this study and implying that the heterogeneous ice formation at $T > -25°C$ is determined by temperature and aerosol load only, biomass burning activities are the outstanding driver of the observed enhanced freezing efficiency in the dry season, even though it is not clear which constituent of the biomass burning aerosol leads to the enhanced ice nucleation efficiency. Solely, the increased presence of black carbon particles, which are known to be rather inefficient ice nuclei, cannot explain the observed freezing efficiency. Observations suggest that the emitted biomass burning aerosol contains in addition fractions of soil dust, combustion ashes, or unmodified pristine organic compounds, such as pollen, bacteria, spores, or organic molecules, which are considered to produce ice much more efficient than pure black carbon particles.

A more thorough investigation of the seasonal difference in the efficiency of ice nucleation in the Amazon Basin by means of in situ observations at cloud level will be required to evaluate the fraction of mineral dust and ice-nucleation-efficient organic compounds of the smoke plumes and to quantify the actual effect of changes in the aerosol properties on heterogeneous freezing efficiency.

References

Althausen, D., R. Engelmann, H. Baars, B. Heese, A. Ansmann, D. Müller, and M. Komppula (2009), Portable Raman lidar Polly[XT] for automated profiling of aerosol backscatter, extinction, and depolarization, *J. Atmos. Oceanic Technol.*, *26*, 2366–2378, doi:10.1175/2009JTECHA1304.1.

Ansmann, A., M. Tesche, P. Seifert, D. Althausen, R. Engelmann, J. Fruntke, U. Wandinger, I. Mattis, and D. Müller (2009), Evolution of the ice phase in tropical altocumulus: SAMUM lidar observations over Cape Verde, *J. Geophys. Res.*, *114*, D17208, doi:10.1029/2008JD011659.

Arana, A., A. L. Loureiro, H. M. J. Barbosa, R. Van Grieken, and P. Artaxo (2014), Optimized energy dispersive X-ray fluorescence analysis of atmospheric aerosols collected at pristine and perturbed Amazon Basin sites, *X-Ray Spectrom.*, *43*(4), 228–237, doi:10.1002/xrs.2544.

Artaxo, P., L. V. Rizzo, J. F. Brito, H. M. J. Barbosa, A. Arana, E. T. Sena, G. G. Cirino, W. Bastos, S. T. Martin, and M. O. Andreae (2013), Atmospheric aerosols in Amazonia and land use change: From natural biogenic to biomass burning conditions, *Faraday Discuss.*, *165*, 203–235, doi:10.1039/C3FD00052D.

Augustin, S., et al. (2013), Immersion freezing of birch pollen washing water, *Atmos. Chem. Phys.*, *13*, 10,989–11,003, doi:10.5194/acp-13-10989-2013.

Baars, H., A. Ansmann, D. Althausen, R. Engelmann, P. Artaxo, T. Pauliquevis, and R. Souza (2011), Further evidence for significant smoke transport from Africa to Amazonia, *Geophys. Res. Lett.*, *38*, L20802, doi:10.1029/2011GL049200.

Baars, H., A. Ansmann, D. Althausen, R. Engelmann, B. Heese, D. Müller, P. Artaxo, M. Paixao, T. Pauliquevis, and R. Souza (2012), Aerosol profiling with lidar in the Amazon Basin during the wet and dry season, *J. Geophys. Res.*, *117*, D21201, doi:10.1029/2012JD018338.

Bühl, J., A. Ansmann, P. Seifert, H. Baars, and R. Engelmann (2013), Toward a quantitative characterization of heterogeneous ice formation with lidar/radar: Comparison of CALIPSO/CloudSat with ground-based observations, *Geophys. Res. Lett.*, *40*, 4404–4408, doi:10.1002/grl.50792.

de Boer, G., H. Morrison, M. D. Shupe, and R. Hildner (2011), Evidence of liquid dependent ice nucleation in high-latitude stratiform clouds from surface remote sensors, *Geophys. Res. Lett.*, *38*, L01803, doi:10.1029/2010GL046016.

DeMott, P. J., et al. (2015), Integrating laboratory and field data to quantify the immersion freezing ice nucleation activity of mineral dust particles, *Atmos. Chem. Phys.*, *15*, 393–409, doi:10.5194/acp-15-393-2015.

Hartmann, S., S. Augustin, T. Clauss, H. Wex, T. Šantl-Temkiv, J. Voigtländer, D. Niedermeier, and F. Stratmann (2013), Immersion freezing of ice nucleation active protein complexes, *Atmos. Chem. Phys.*, *13*, 5751–5766, doi:10.5194/acp-13-5751-2013.

Hoose, C., and O. Möhler (2012), Heterogeneous ice nucleation on atmospheric aerosols: A review of results from laboratory experiments, *Atmos. Chem. Phys.*, *12*, 9817–9854, doi:10.5194/acp-12-9817-2012.

Kanitz, T., P. Seifert, A. Ansmann, R. Engelmann, D. Althausen, C. Casiccia, and E. G. Rohwer (2011), Contrasting the impact of aerosols at northern and southern midlatitudes on heterogeneous ice formation, *Geophys. Res. Lett.*, *38*, L17802, doi:10.1029/2011GL048532.

Korolev, A. V., and I. P. Mazin (2003), Supersaturation of water vapor in clouds, *J. Atmos. Sci.*, *60*(24), 2957–2974, doi:10.1175/1520-0469(2003)060<2957:SOWVIC>2.0.CO;2.

Kulmala, M., et al. (2011), General overview: European Integrated Project on Aerosol Cloud Climate and Air Quality interactions (EUCAARI)—Integrating aerosol research from nano to global scales, *Atmos. Chem. Phys.*, *11*, 13,061–13,143, doi:10.5194/acp-11-13061-2011.

Lenton, T. M., H. Held, E. Kriegler, J. W. Hall, W. Lucht, S. Rahmstorf, and H. J. Schellnhuber (2008), Tipping elements in the Earth's climate system, *Proc. Natl. Acad. Sci.*, *105*(6), 1786–1793, doi:10.1073/pnas.0705414105.

Martin, S. T., et al. (2010), An overview of the Amazonian Aerosol Characterization Experiment 2008 (AMAZE-08), *Atmos. Chem. Phys.*, *10*, 11,415–11,438, doi:10.5194/acp-10-11415-2010.

Morcrette, J.-J., et al. (2009), Aerosol analysis and forecast in the European Centre for Medium-Range Weather Forecasts Integrated Forecast System: Forward modeling, *J. Geophys. Res.*, *114*, D06206, doi:10.1029/2008JD011235.

Murray, B. J., D. O'Sullivan, J. D. Atkinson, and M. E. Webb (2012), Ice nucleation by particles immersed in supercooled cloud droplets, *Chem. Soc. Rev.*, *41*, 6519–6554, doi:10.1039/C2CS35200A.

Nisantzi, A., R. E. Mamouri, A. Ansmann, and D. Hadjimitsis (2014), Injection of mineral dust into the free troposphere during fire events observed with polarization lidar at Limassol, Cyprus, *Atmos. Chem. Phys.*, *14*(22), 12,155–12,165, doi:10.5194/acp-14-12155-2014.

Pöschl, U., et al. (2010), Rainforest aerosols as biogenic nuclei of clouds and precipitation in the Amazon, *Science*, *329*, 1513–1516, doi:10.1126/science.1191056.

Prenni, A. J., M. D. Petters, S. M. Kreidenweis, C. L. Heald, S. T. Martin, P. Artaxo, R. M. Garland, A. G. Wollny, and U. Pöschl (2009), Relative roles of biogenic emissions and Saharan dust as ice nuclei in the Amazon Basin, *Nat. Geosci.*, *2*, 402–405, doi:10.1038/ngeo517.

Sassen, K., P. J. DeMott, J. M. Prospero, and M. R. Poellot (2003), Saharan dust storms and indirect aerosol effects on clouds: CRYSTAL–FACE results, *Geophys. Res. Lett.*, *30*, 1633, doi:10.1029/2003GL017371.

Seifert, P., A. Ansmann, I. Mattis, U. Wandinger, M. Tesche, R. Engelmann, D. Müller, C. Pérez, and K. Haustein (2010), Saharan dust and heterogeneous ice formation: Eleven years of cloud observations at a central European EARLINET site, *J. Geophys. Res.*, *115*, D20201, doi:10.1029/2009JD013222.

Seifert, P., et al. (2011), Ice formation in ash-influenced clouds after the eruption of the Eyjafjallajökull volcano in April 2010, *J. Geophys. Res.*, *116*, D00U04, doi:10.1029/2011JD015702.

Umo, N. S., B. J. Murray, M. T. Baeza-Romero, J. M. Jones, A. R. Lea-Langton, T. L. Malkin, D. O'Sullivan, J. M. C. Plane, and A. Williams (2015), Ice nucleation by combustion ash particles at conditions relevant to mixed-phase clouds, *Atmos. Chem. Phys.*, *15*, 5195–5210, doi:10.5194/acp-15-5195-2015.

Westbrook, C. D., and A. J. Illingworth (2011), Evidence that ice forms primarily in supercooled liquid clouds at temperatures $> -27°$C, *Geophys. Res. Lett.*, *38*, L14808, doi:10.1029/2011GL048021.

Zhang, D., Z. Wang, A. Heymsfield, J. Fan, D. Liu, and M. Zhao (2012), Quantifying the impact of dust on heterogeneous ice generation in midlevel supercooled stratiform clouds, *Geophys. Res. Lett.*, *39*, L18805, doi:10.1029/2012GL052831.